

## ESTABLISHMENT AND EXPERIMENTAL VERIFICATION OF THE HOOP TENSION MECHANICAL MODEL OF ALUMINUM ALLOY TUBE

by

**Xiaohua CHEN\***, **Zhanshan WANG**, **Yan YANG**, and **Guangcai ZHANG\***

Department of Mechanical and Electrical Engineering,  
Suzhou Vocational Institute of Industrial Technology, Suzhou, China

Original scientific paper  
<https://doi.org/10.2298/TSCI190508068C>

*The ring hoop tension test is an important test method for evaluating the deformation performance of tube. The mechanical model of the hoop tension test is established under the condition that deformation caused by the friction of the die is unequal. The mechanical model is input into the finite element model and compared with the tube uniaxial hoop tensile test. The mechanical model simulation obtained by this method has a better coincidence with the experimental data. Through further analysis of the bulging test of the process, it is proved that the established hoop mechanical model can accurately reflect the plasticity variation characteristics of the tube deformation.*

Key words: ring hoop tension test, aluminum alloy, finite element analysis

### Introduction

Generally, the method for obtaining the properties of the tube material is a uniaxial tensile test. But the analysis of the tube bulging process using the data obtained by the axial tensile test will bring a large error. In order to obtain the hoop deformation performance of the tube, the test method of the hoop tension came into being. Since Arsene and Bai [1] proposed the hoop tensile test process in 1996. Dick [2-5] designed a set of circumferential unidirectional test fixtures. The digital image method was used to observe the change of strain field in the gauge section of the ring specimen during deformation. He [6] through the hoop tensile test shows that the bulging performance of magnesium alloy AZ31 tube in the hot state is better than normal temperature. He *et al.* [7] and Zha [8] analyzed the mechanical analysis of the uniaxial hoop tensile test, when the position of the hoop gauge segment was 90° from the horizontal direction, the D-shaped block of the gauge length segment has the smallest frictional force and the maximum circumferential pulling force. It can be seen from the above research results that during the axial tensile test, the friction between the material and the mold causes uneven deformation of the gauge length of the test specimen, which brings great error to the calculation of the test data and the calculation of the material properties.

In this paper, the mechanical model of the hoop tensile test process is established under the condition of uneven deformation caused by the friction of the mold, and the model is mathematically processed by the parameter fitting method to obtain the hoop deformation of

\* Corresponding author, e-mail: cxh05123@163.com

the tube. The performance and the corresponding bulging process test were carried out to verify the hoop mechanics model.

**Hoop tension test process and deformation analysis of test specimen**

The mold for the ring hoop tension test (RHTT) consists of two D-shaped blocks [8], and the shape is as shown in fig. 1. During the test, the D-shaped block at the lower end is fixed, and the D-shaped block at the upper end is displaced in the y-axis direction under the action of the traction force  $P$ . The  $P$ - $S$  curve, as shown in fig. 1. The geometric relationship between the deformation of the specimen before and after deformation is shown in fig. 2. According to the geometric relationship shown in the figure, the elongation before and after deformation of the test specimen can be calculated.

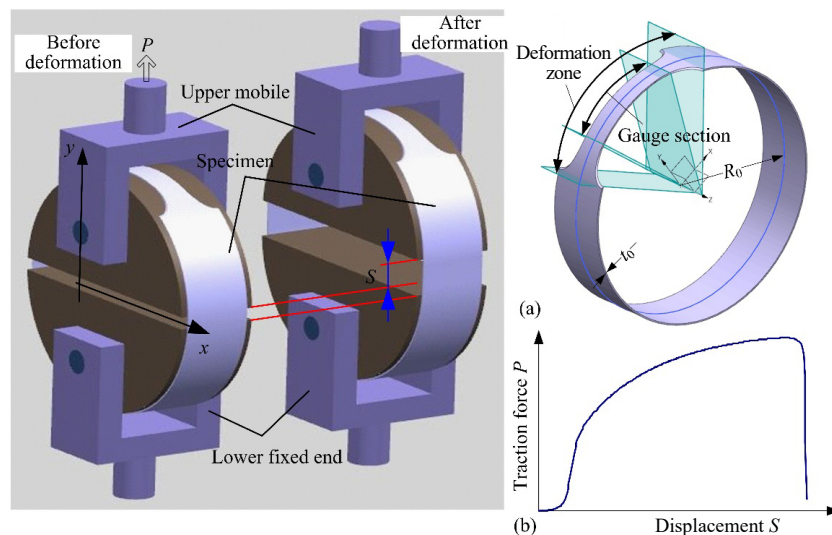


Figure 1. The RHTT: (a) ring specimen, (b) figure  $P$ - $S$

The length of the whole specimen before and after deformation is, respectively:

$$C_0 = 2\pi R_0 \quad C = 2S + 2S_0 + 4R_0 \arcsin\left(\frac{L_D}{2R_0}\right) \tag{1}$$

where  $R_0$  is the radius of the ring specimen,  $L_D$  – the horizontal end length of the D-shaped block, and  $S_0 = 2[R_0^2 - (L_D/2)^2]^{1/2}$ .

Therefore, the elongation of the test specimen is:

$$\Delta C = 4R_0 \arcsin\left(\frac{L_D}{2R_0}\right) - 2\pi R_0 + 2S + 2S_0 \tag{2}$$

**Mechanical equilibrium analysis**

*Solution of hoop tension*

During the tensile process of the RHTT specimen, the test specimen is cut in half along the middle section of the upper and lower D-shaped blocks, and the force state is as

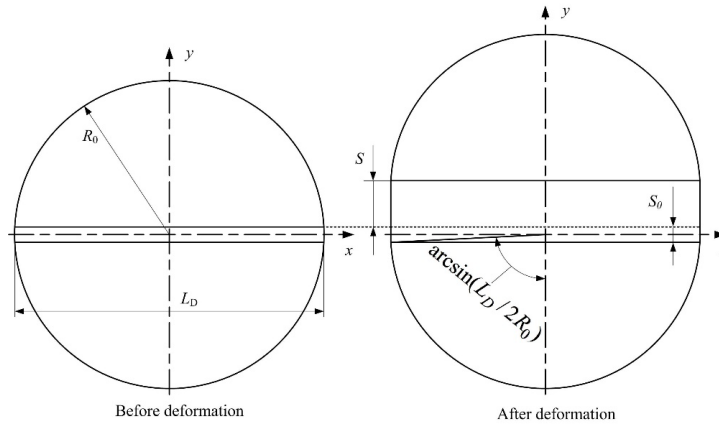


**Figure 2. Deformation geometry relation of ring specimen**

shown in fig. 3. The force unit is cut at any position on the test specimen, and the radial and circumferential force balance is obtained:

$$F(\theta) \sin \frac{d\theta}{2} + [F(\theta) + dF] \sin \frac{d\theta}{2} - N(\theta) = 0 \quad (3)$$

$$F(\theta) \cos \frac{d\theta}{2} - \mu N(\theta) - [F(\theta) + dF] \cos \frac{d\theta}{2} = 0 \quad (4)$$

where  $F(\theta)$  is the hoop  $t$  of the unit, and  $N(\theta)$  is the supporting force of the D-shaped block to the unit.

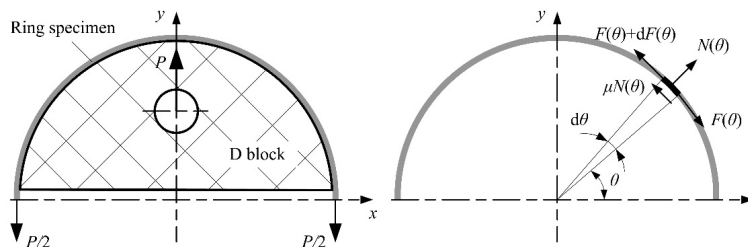


**Figure 3. Stress analysis of ring hoop tension**

When  $\theta$  is very small,  $\sin(d\theta/2) = 1/2d\theta$ ,  $\cos(d\theta/2) = 1$ , combined differential equation, from the balance of the forces in fig. 3, the boundary condition is: when  $\theta = 0$ ,  $F(\theta) = P/2$ , the constant  $c = -\ln(P/2)$  can be determined. The tension of the specimen is satisfied:

$$F(\theta) = \frac{P}{2 \exp(-\mu\theta)} \quad (5)$$

where  $P$  is the tensile force of the D-shaped block and  $\mu$  – the friction coefficient between the test specimen and the D-shaped block.

#### Material parameter solving model

The deformation part of the hoop tensile test specimen is divided into  $m$  parts, each part is a unit, and the specimens during the test is placed in the deformation position with re-

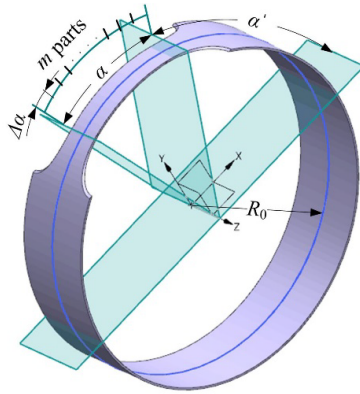


**Figure 4. Ring specimen deformation zone division**

spect to the  $y$ -axis. The central angle of the total length of the deformation zone is  $\alpha$ , the corresponding central angle of each part is  $\Delta\alpha$ , and the angle between the outermost edge and the  $x$ -axis is  $\alpha'$ , fig. 4. During the deformation process, each unit undergoes elongation deformation under the direction of tension. Therefore, each unit is in a unidirectional stress state. According to the analysis of hoop tension, the hoop tensile stress and the hoop strain of the  $i^{\text{th}}$  element are:

$$\sigma_{\theta i} = \frac{F(\theta)|_{\theta=\alpha'+(i-1)\Delta\alpha}}{B_i t_i} \quad \varepsilon_{\theta i} = \ln \frac{l_i}{l_0} \quad (6)$$

where  $B_i$ ,  $t_i$ ,  $l_i$  are respectively the width, thickness and length of the  $i^{\text{th}}$  unit after deformation,  $B_0$ ,  $t_0$ ,  $l_0$  are the width, thickness and length of each unit before deformation.

Obtained by constant volume conditions:

$$B_i t_i l_i = B_0 t_0 l_0 \quad (7)$$

Ignore the elastic deformation, and assume that the plastic stress-strain hardening relationship of the material satisfies the exponential hardening model:  $\sigma = K\varepsilon^n$ , and considering the uniaxial stress state  $\sigma_{\theta i} = \sigma$ ,  $\varepsilon_{\theta i} = \bar{\varepsilon}$ , so the eqs. (5)-(7) can be substituted into the material model formula:

$$\frac{P l_i \exp[-\mu\alpha' - \mu(i-1)\Delta\alpha]}{2B_0 t_0 l_0} = K \left( \ln \frac{l_i}{l_0} \right)^n \quad (8)$$

The length of each unit after deformation can be inversely solved by eq. (8), However, limited to the eq. (8) is complex, the explicit analytic expression of  $l_i$  cannot be obtained, and temporarily use an implicit function  $l_i = f(P)$  for  $P$  to represent:

The elongation of the gauge length is:

$$\Delta L = \sum_{i=1}^m l_i - \alpha R_0 \quad (9)$$

Since the gauge length of the test specimen is narrower than the other parts, the deformation of the test specimen during the stretching process is mainly concentrated in this part. If the elongation caused by deformation of other parts besides the gauge section is slightly removed, it can be considered that the elongation of the specimen is equal to that of the gauge section ( $\Delta L = \Delta C$ ). Thus:

$$\sum_{i=1}^m f(P) - \alpha R_0 + 2\pi R_0 - 2S - 2S_0 - 4R_0 \arcsin\left(\frac{L_D}{2R_0}\right) = 0 \quad (10)$$

By using the data points acquired, the two parameters  $K$ ,  $n$  in the fitting eq. (10) can be obtained, thus the material performance parameters can be obtained. The MATLAB math software can be used to perform the fitting process and the explicit function of the implicit equation.

**Tensile test and finite element simulation verification**

High-strength aluminum alloy tube is poorly plastic at room temperature. The plastic deformation of thin tubes is usually achieved by warm forming [9] or immediately forming after solution treatment [10, 11]. Based on the previous research [12], the material forming quality and plastic forming properties of the material at 190 °C is optimal, the parameters used in the tests are shown in tab. 1. The P-S curve measured by the test is shown in fig. 5(a), and the material performance parameters obtained by fitting are shown in tab. 2.

**Table 1. Known variable parameter values for the ring hoop tension test**

Test known variables	D-shaped block straight side length $L_D$ [mm]	D-block radius $R_0$ [mm]	Initial thickness of specimen $t_0$ [mm]	Initial width of gauge segment $B_0$ [mm]	Pitch angle $\alpha$ [rad]	Angle between the edge of the gauge length and the x-axis $\alpha'$ [rad]	The number of units in the gauge length segment is $m$
Variable value	99.87	50.00	1.20	10.00	0.70	0.93	50.00

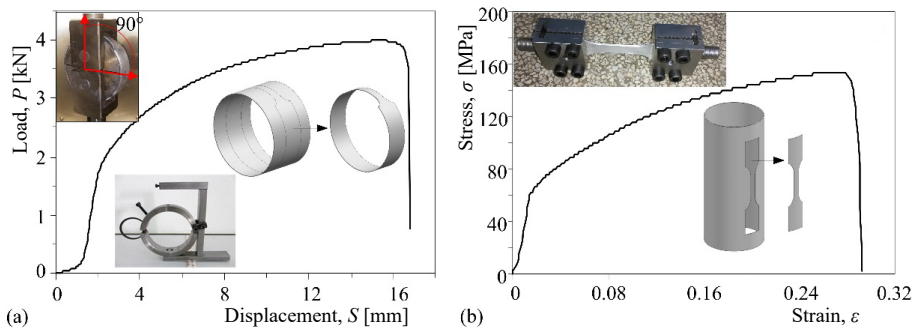


**Figure 5. The RHTT of aluminum: (a) ring hoop tensile load displacement curve, (b) axial tensile stress-strain curve**

The main chemical components of tube are shown in tab. 3. At the same time, the uni-directional tensile tests were carried out on the standard tensile specimens cut along the axial direction. The true stress-strain curve obtained by the uniaxial tensile test is shown in fig. 5(b), and the material performance parameters are shown in tab. 2.

**Table 2. Material's mechanical properties**

Material performance parameters	Hoop tensile test	Axial tensile test
Strength coefficient, $K$ [Mpa]	275.02	307.93
Hardening index, $n$	0.2553	0.3316

**Table 3. Chemical composition of aluminum alloy tube**

Si	Mg	Cu	Fe	V	Ti	Cr	Ga	Zn	Mn	Ni	Al
0.815	0.181	0.136	0.08	0.023	0.019	0.011	0.01	0.083	0.054	0.051	Rem

In this paper, considering the uneven deformation caused by friction during the hoop tension, the deformation process of the hoop specimen is mechanically modeled, and the plastic strain hardening parameters of the material are obtained by the inverse fitting method. The results obtained by this method can whether it accurately reflects the hoop hardening performance of the tube needs further research. Based on the previous two points, the finite element simula-

tion of the hoop tensile test process is carried out, and the *load-displacement* historical output of the D-shaped block is extracted to compare with the test results to evaluate the accuracy of the material model.

The comparison between simulation and experiment is shown in fig. 6(b). It can be seen that the plastic hardening performance of the tube used in this paper is different in the hoop direction and axial direction. The hardening properties obtained by fitting the mechanical model in this paper can more accurately reflect the hoop properties of the tube. In order to further verify the accuracy of the hoop mechanical model, the corresponding tube bulging test is carried out.

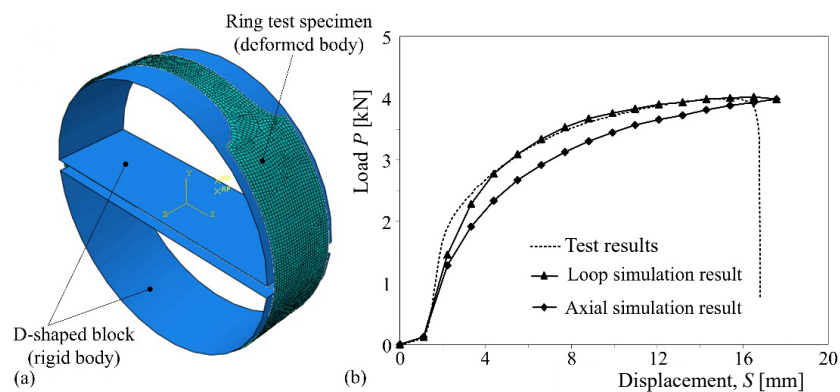


Figure 6. Finite element simulation model and simulation results: (a) simulation model, (b) comparison of simulation results with tests

### Tube forming simulation and process test

The non-metallic granules (NMG) medium pressure forming process is an extension of the high pressure forming technology in the tube [13]. The  $ZrO_2$  and  $SiO_2$  were selected as the medium components in the process test. The particle size between 0.22-0.38 mm, and the appearance is smooth and rounded to a hardness of 48-55HRC, which is a discrete non-stick material [14-16]. The extended Drucker-Prager linear material model in

Table 4. Drucker-Prager linear model parameters of NMG media ( $t = 190\text{ }^\circ\text{C}$ )

Friction angle in medium, $\beta$ [ $^\circ$ ]	Stress ratio, $\chi$	Dilation angle, $\psi$ [ $^\circ$ ]	External friction factor, $\mu_n$
34.1	0.82	17.5	0.2

geotechnical mechanics can be used to express the mechanical properties of granular media under monotonic loading conditions [17]. The extended Drucker-Prager material parameters at  $190\text{ }^\circ\text{C}$  are shown in tab. 4.

In order to ensure the accuracy of the simulation results, the NMG medium and the tube mesh are given adaptive function, the thick anisotropy of the tube is ignored. Seven integral points are selected in the thickness direction, and the penalty function contact algorithm is used between the contact surfaces. The length of the bulging zone and the radius of the fillet of the die are based on the actual process tests, which are 30 mm and 6 mm, respectively (as shown in fig. 7).

Figure 8 is an experimental device for tube thermal bulging. The initial length of the tube blank is  $l_0 = 90\text{ mm}$ . As the head force increases, the bulging diameter of the free forming area of tube increases. When the indenter force  $F = 230\text{ kN}$ , the bulging profile and wall thickness of the tube are changed uniformly, when the indenter force reaches  $F = 250\text{ kN}$ , the bulging

zone of the tube is broken along the axial direction, showing obvious ductile fracture characteristics.

When the indenter force is  $F = 230$  kN, the analysis shows that the simulation of the tube and the wall thickness distribution of the test are the same is shown in Figure 8. In the forming zone, the measured wall thickness is larger than the simulated wall thickness, and the minimum measured wall thickness is 1.25 mm. Compared with the minimum simulated wall thickness of 1.24 mm in the

same process scheme, the increase is 0.01 mm, and the error is basically within 5%. The measured wall thickness at the upper and lower fillets is smaller than the simulated wall thickness value, which is related to the complex mechanical properties of the granular media in the process [18]. Therefore, it is proved that the established hoop mechanical model can accurately reflect the mechanical changes of the tube during plastic deformation.

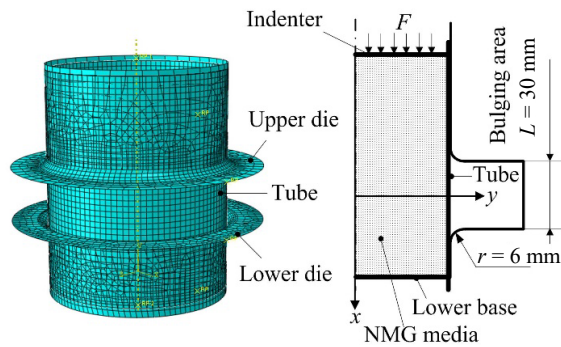


Figure 7. Finite element model of bulging process

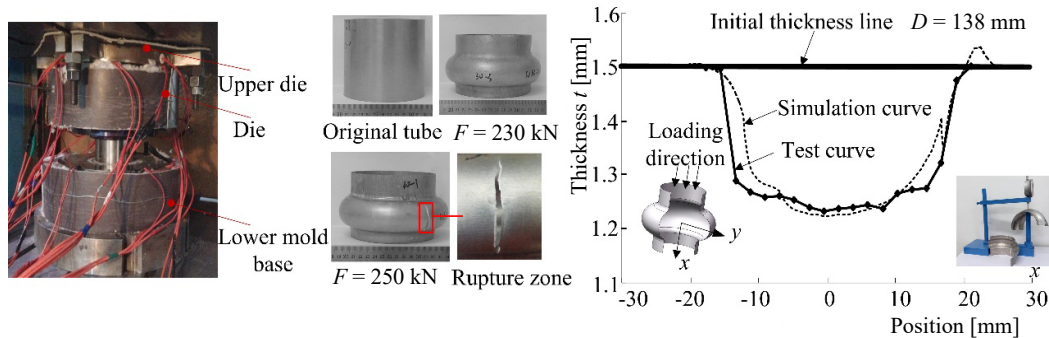


Figure 8. Contrasting curves of wall thickness between process test and FEM

## Conclusions

- According to the mechanical model established in this paper, the data of the hoop tensile test is processed by the inverse fitting method. The strength coefficient,  $K$ , and the hardening exponent  $n$  in the exponential hardening model ( $\sigma = K\varepsilon_n$ ) can be used to evaluate the hoop hardening property of tube very well.
- The bulging test of the tube hot NMG process shows that the simulation and test wall thickness distribution of tube are the same, and the error is less than 5%. It is proved that the established hoop mechanical model can accurately reflect the plasticity change characteristics of tube deformation.

## References

- [1] Arsene, S., Bai. J.. A New Approach to Measuring Transverse Properties of Structural Tubing by a Ring Test, *Journal of Testing and Evaluation*, 26 (1998), 1, pp. 26-30
- [2] Dick, C. P., Korkolis, Y. P., Mechanics and Full-Field Deformation Study of the Ring Hoop Tension Test, *International Journal of Solids and Structures*, 51 (2014), 18, pp. 3042-3057
- [3] Dick, C. P., Korkolis, Y. P., Assessment of Anisotropy of Extruded Tubes by Ring Hoop Tension Test, *Procedia Engineering*, 81 (2014), Dec., pp. 2261-2266

- [4] Dick, C. P., Korkolis, Y. P., Strength and Ductility Evaluation of Cold-Welded Seams in Aluminum Tubes Extruded Through Porthole Dies, *Material and Design*, 67 (2015), Feb., pp. 631-636
- [5] Korkolis, Y. P., et al., Formability Assessment of Al-6xxx-T4 Tubes for Hydroforming Applications, *Proceedings*, SAE World Congress, Detroit, Mich., USA, 2013
- [6] He, Z. B., et al., Formability Testing of AZ31B Magnesium Alloy Tube at Elevated Temperature, *Journal of Materials Processing Technology*, 210 (2010), 6-7, pp. 877-884
- [7] He, Z. B., et al., Force and Deformation Analysis of Tube Ring Specimen During Hoop Tension Test, *Acta Metallurgica Sinica*, 44 (2008), 4, pp. 423-427
- [8] Zha, W. W., Ring Tensile Test Method for Mechanical Properties of Magnesium Alloy Tube, M. Sc. thesis, Harbin University of Technology, Harbin, China, 2007
- [9] He, Z., et al., Formability and Microstructure of AA6061 Al Alloy Tube for Hot Metal Gas Forming at Elevated Temperature, *Transaction of Nonferrous Metals Society of China*, 22 (2012), Suppl. 2, pp. S364-S369
- [10] Bi, J., et al., Heat Treatment and Granule Medium Internal High-Pressure Forming of AA6061 tube, *Journal of Central South University*, 24 (2017), June, pp. 1040-1049
- [11] Liu, G., et al., Warm Hydroforming of Magnesium Alloy Tube with Large Expansion Ratio Within Non-Uniform Temperature Field, *Transactions of Nonferrous Metals Society of China*, 22 (2012), 11, pp. 408-415
- [12] Chen, X. H., et al., Analyses of AA5083 Tube Warm Bulging Processes under Non-Uniform Pressures of Granule Medium, *China Mechanical Engineering*, 27 (2016), 24, pp. 3375-3381
- [13] Chen, H., et al., Granular Media-Based Tube Press Hardening, *Journal of Materials Processing Technology*, 228 (2016), Feb., pp. 145-159
- [14] Esteban, M., et al., Bifurcation Analysis of Hysteretic Systems with Saddle Dynamics, *Applied Mathematics & Nonlinear Sciences*, 2 (2017), 2, pp. 449-464
- [15] Bortolan, M, C., Rivero, F., Non-Autonomous Perturbations of a Non-Classical Non-Autonomous Parabolic Equation with Subcritical Nonlinearity, *Applied Mathematics & Nonlinear Sciences*, 2 (2017), 1, pp. 31-60
- [16] Chen, X. H., et al., Formability of Hot Non-Metallic Granule Medium of AA5083 Aluminum Alloy Tube under Various Loading Paths, *China Mechanical Engineering*, 27 (2016), 18, pp. 2547-2555
- [17] Dong, G. J., et al., Stress-Strain Analysis on AA7075 Cylindrical Parts during Hot Granule Medium Pressure Forming, *Journal of Central South University*, 23 (2016), 11, pp. 2845-2857
- [18] Dong, G. J., et al., Research on AA6061 Tubular Components Prepared by Combined Technology Heat Treatment and Internal High Pressure Forming, *Journal of Materials Processing Technology*, 242 (2017), Apr., pp. 126-138